

ExMAG: Learning of Maximally Ancestral Graphs

Petr Ryšavý¹, Pavel Rytíř¹, Xiaoyu He¹, Jakub Mareček¹, and Georgios Korpas^{2,1,3}

¹Department of Computer Science, Czech Technical University in Prague, Czech Republic

²HSBC Quantum Technologies Group, Innovation & Ventures, HSBC, Singapore

³Archimedes Research Unit on AI, Data Science and Algorithms, Marousi, Greece

March 12, 2025

Abstract

As one transitions from statistical to causal learning, one is seeking the most appropriate causal model. Dynamic Bayesian networks are a popular model, where a weighted directed acyclic graph represents the causal relationships. Stochastic processes are represented by its vertices, and weighted oriented edges suggest the strength of the causal relationships. When there are confounders, one would like to utilize both oriented edges (when the direction of causality is clear) and edges that are not oriented (when there is a confounder), yielding mixed graphs. A little-studied extension of acyclicity to this mixed-graph setting is known as maximally ancestral graphs.

We propose a score-based learning algorithm for learning maximally ancestral graphs. A mixed-integer quadratic program is formulated, and an algorithmic approach is proposed, in which the pre-generation of exponentially many constraints is avoided by generating only violated constraints in the so-called branch-and-cut (“lazy constraint”) method. Comparing the novel approach to the state-of-the-art, we show that the proposed approach turns out to produce more accurate results when applied to small and medium-sized synthetic instances containing up to 25 variables.

1 Introduction

Simpson’s paradox is not a paradox, but empirically analysing causality without considering confounding factors in statistical analysis[28]. An interesting example is the Berkeley graduate admission paradox. The data show that women face higher difficulties when applying to graduate schools. Nevertheless, the reason is that women tend to apply to popular departments. In this example, academic ability can be a potential confounder since ability could influence the choice of department and the probability of admission. Controversially, [26] analyzed gene expression data from both human and mouse samples and concluded that data cluster more by tissue rather than by species. Within one year of the publication, [17] quickly realized that the previous paper integrated both previously published and newly collected human and mouse gene expression data without eliminating batch effects, which significantly caused the wrong results. The batch effect, stemming from different labs and sample processing protocols, was a key confounder that distorted the apparent species-based clustering of gene expression. Addressing this confounding variable through correction (using ComBat) revealed that tissue, not species, was the primary driver of gene expression patterns, emphasizing the importance of recognizing confounders in causal analysis. Therefore, recognizing and controlling for these confounders is crucial to avoid drawing incorrect conclusions about causality.

Meanwhile, confounders represent a significant challenge in the process of causal inference, as they can cause catastrophe in discovering the relationships between observed variables across various fields. In the fields of financial econometrics, hidden states, such as regional heterogeneity, economic policy, or unobserved individual characteristics, can be addressed by using Difference-in-Differences (DiD) [15], Instrumental variables (IV) and Mendelian randomization (MR) to avoid incorrect conclusions about risk and returns [23]. Significantly, in biomedical science, confounders such as socio-economic status, age, or lifestyle factors can distort the true causal relationship between treatments and outcomes. Techniques such as propensity score matching [35] and instrumental variable approaches have been widely used to mitigate the effects of confounding in clinical trials and observational studies. In bioinformatics, particularly in genome-wide association studies (GWAS), confounders, including population stratification

and environmental exposures, must be controlled to avoid biased estimates in genetic association studies [8, 18]. To mitigate such biases, statistical models that explicitly account for hidden confounders, such as spectral methods and latent variable models, are often employed [18]. Furthermore, meta-analysis and sensitivity analysis are often employed to evaluate the robustness of findings in the presence of potential confounders, especially when combining results from multiple studies [5, 27]. These methodologies ensure that the conclusions drawn are reliable and actionable, improving the credibility of statistical models across disciplines.

In previous research, the effects of hidden bias in high-dimensional settings have been neglected. In [7] were confounders first given significant attention. Subsequently, this method leverages the dominant eigenstructure of time series to separate confounding influences and demonstrates that the performance of the estimation may improve as the dimension of the time series increases [25]. Recently, more statistical research has been introduced to enhance causal inference. Anchor regression, for instance, bridges the gap between causality and robustness by addressing heterogeneity in data [36]. Other significant contributions include spectral deconfounding, a technique designed to mitigate the effects of hidden confounders in high-dimensional settings [6]. This approach provides a framework for robust predictions in the presence of shifts in data distributions. Similarly, the invariance principle has emerged as a cornerstone of causal inference, linking causal structure to robust statistical models [5]. Furthermore, the concept of doubly robust inference offers an alternative framework for addressing hidden confounding factors, combining model robustness with efficiency in high-dimensional scenarios [18]. Together, these developments represent a significant leap forward in understanding and addressing the challenges posed by complex causal systems.

While previous work has focused primarily on constructing optimal Directed Acyclic Graphs (DAGs), these models have limitations when it comes to incorporating cycles and latent variables. On the other hand, Maximal Ancestral Graphs (MAGs) allow for more flexibility by accommodating both direct and indirect relationships among variables, even in the presence of confounding factors. In particular, MAGs can represent feedback loops and bidirectional relationships that DAGs cannot, making them a more powerful tool for capturing the complex dynamics of real-world causal systems. There are two classic types of graphical learning algorithms for constructing causal models: constraint-based and score-based methods, and sometimes hybrid methods that combine the first two approaches is considered as the third type. The canonical constraint-based method for learning DAGs (directed acyclic graphs) and DAGs (directed acyclic graphs) graphs are the PC and FCI algorithm, separately [39]. This type of method works magically in a way that conditional independences can be tested by statistical methods, and the graph can be reconstructed accordingly. However, a key limitation of constraint-based methods is that when the group of variables is large, errors in conditional independence tests tend to occur more often. Such errors will be caused in graph construction and mislead to a wrong causal relationship representing the data [31, 14].

Existing approaches to scoring ADMGs often rely on numerical methods for MLE estimation, as closed-form solutions are unavailable [32]. Additionally, factorization in ADMGs is not directly decomposable into individual variables and their parent sets, as in DAGs, but must instead consider components connected by bidirected paths (termed *districts* or *c-components*). The significant computational challenge of score-based methods is time-consuming, that is due to the number of graphs visited. In this way, [9] proposed that the Markov equivalence class (MEC) can be deployed to minimize scoring graphs in the visited MEC again. Our approach emphasizes the integration of MAGs with the recognition of confounders, offering a more accurate representation of causal relationships, as well as a more efficient method. By identifying the optimal MAG through Mixed-Integer Nonlinear Programming (MINLP), we can ensure that confounding factors are properly accounted for and that the resulting causal model reflects the true underlying data-generating process.

1.1 Motivating Example

Berkeley graduate admission paradox is famous in statistical teaching to illustrate Simpson’s paradox. Like most paradoxes, there is no violation of logic, just of intuition. And since different people have different intuitions, Simpson’s paradox means different things to different people. The poor intuition being violated in this case is that a positive association in the entire population should also be held within each department. Overall, females in these data did have a harder time getting admitted to graduate school. But that arose because females applied to the hardest departments for anyone, male or female, to gain admission to.

Perhaps a little more paradoxical is that this phenomenon can repeat itself indefinitely within a sam-

ple. Therefore, we proved that our method ExMAG is sufficient in revealing the true causal influence or rather just identifying confounders of the Berkeley graduate admission paradox example. The admission probabilities were modeled using the binomial Bayesian framework, and the posterior is approximated when priors are assigned, as illustrated in the notebook in supplementary materials.

2 Graphs and Properties

Maximal ancestral graphs (MAGs), first introduced by [33], provide a framework for modeling distributions through conditional independence (CI) relations. Compared with directed acyclic graphs (DAGs), MAGs release the assumption of no latent confounders, accommodating data that arises from distributions with more complex independent structures and revealing hidden states in the graphs. These graphs have demonstrated their utility in a variety of contexts, such as inferring causal effects from observational data. While DAGs allow efficient computation of maximum likelihood estimates (MLEs) and scoring (e.g., via BIC), these properties are challenging to extend to ADMGs due to their structural and computational complexity [21].

ADMG One can illustrate any causal relationship as an acyclic directed mixed graph (ADMG), which is acyclic and contains only two types of edges: directed (\rightarrow) and bidirected (\leftrightarrow). A graph \mathcal{G} , which consists of a vertex set \mathcal{V} and an edge set \mathcal{E} of pairs of distinct vertices, is acyclic if there does not exist any sequence of vertices v_0, v_1, \dots, v_k (with $k \geq 1$) such that:

$$\forall i \in \{0, \dots, k-1\}, (v_i, v_{i+1}) \in E \quad \text{and} \quad (v_k, v_0) \in E.$$

In other words, an acyclic \mathcal{G} contains no directed cycles.

For an edge in \mathcal{E} connecting vertices a and b , we say these two vertices are the *endpoints* of the edge and the two vertices are *adjacent* (if there is no edge between a and b , they are *nonadjacent*). For a vertex v in an ADMG \mathcal{G} , we define the *parents*, *siblings*, *ancestors*, and *district* of v , respectively as:

$$\begin{aligned} \text{pa}_G(v) &= \{w : w \rightarrow v \text{ in } G\}, \\ \text{sib}_G(v) &= \{w : w \leftrightarrow v \text{ in } G\}, \\ \text{an}_G(v) &= \{w : w \rightarrow \dots \rightarrow v \text{ in } G \text{ or } w = v\}, \\ \text{dis}_G(v) &= \{w : w \leftrightarrow \dots \leftrightarrow v \text{ in } G \text{ or } w = v\}. \end{aligned}$$

m-separation For an ADMG \mathcal{G} , given a subset $W \subseteq \mathcal{V}$, the induced subgraph G_W is defined as the graph with vertex set W and edges in \mathcal{G} whose endpoints are both in W . Also for the district of a vertex v in an induced subgraph G_W , we may denote it by $\text{dis}_W(v) = \text{dis}_{G_W}(v)$.

Graphs are associated with conditional independence relations via a separation criterion; in the case of ADMGs, we use m-separation. Graphs encode conditional independence relations through separation criteria. For ADMGs, *m-separation* is used, which generalizes d-separation for DAGs to account for bidirected edges. A path between two vertices a and b is *m-connecting* given a conditioning set $C \subseteq \mathcal{V}$ if:

1. a and b are endpoints of the path;
2. Every noncollider on the path is not in C ;
3. Every collider is in $\text{an}_G(C)$.

Graphs that encode the same set of CI relations are said to belong to the same MEC. This equivalence class structure is critical for reducing redundancy during graph exploration and scoring.

MAG An ADMG \mathcal{G} is called a maximal ancestral graph (MAG) if:

- (i) For every pair of nonadjacent vertices a and b , there exists some set C such that a, b are *m-separated* given C in \mathcal{G} (*Maximality*);
- (ii) For every $v \in \mathcal{V}$, $\text{sib}_G(v) \cap \text{an}_G(v) = \emptyset$ (*Ancestrality*).

We refer to [20] for multiple examples.

3 Brief Introduction To Mixed Integer Quadratic Programming

Let us also provide a short introduction to mixed-integer quadratic programming. An optimization problem is called a mixed-integer quadratically constrained quadratic program (MIQCQP) if it is of the form

$$\min_{x \in \mathbb{R}^n} x^T Q x + q^T x, \quad (1)$$

$$\text{s.t. } x^T Q_i x + q_i^T x \leq a_i, \quad (2)$$

$$A x \leq b, \quad (3)$$

$$x \in F \quad (4)$$

where $Q, Q_i \in \mathbb{R}^{n,n}$, $q, q_i \in \mathbb{R}^n$, $A \in \mathbb{R}^{m,n}$, $a \in \mathbb{R}^k$, $b \in \mathbb{R}^m$, F is a product of the form

$$F = \underbrace{\mathbb{R} \times \dots \times \mathbb{R}}_{n-r \text{ times}} \times \underbrace{\mathbb{N} \times \dots \times \mathbb{N}}_{r \text{ times}} \quad (5)$$

and $m, n, k, r \in \mathbb{N}$. Equation (1) is often called the cost or loss function, (2) represents the quadratic constraints, (3) are the linear constraints, and F is the set that enforces the integrality constraints for the r components of the decision variable x .

Mixed-integer quadratic programs have been shown to be NP-hard [12], which often leads to an exhaustive demand for computational resources. The algorithms used to solve MIQP are typically branch-and-bound or cutting plane [10, 4, 40, 24]. Both of these algorithmic treatments are often employed together, often with the addition of a presolving step, the use of heuristics, and parallelism. The aforementioned allows many modern solvers to solve even large problems despite the NP-hardness. Some of these solvers are open source (like SCIP and GLPK), and others are commercial (GUROBI and CPLEX). The powerful infrastructure present in these solvers can be made use of together with additional problem-specific modifications to deliver high-quality solutions.

Due to the exhaustive nature of the algorithms mentioned in the previous paragraph, global convergence is guaranteed [2]. Furthermore, convergence to the global solution may be tracked, and the error estimated by computing the dual problem of (1–4). The dual of the problem is then used to compute the so-called MIP GAP as follows

$$\text{MIP GAP} = \frac{|J(x^*) - J_{\text{dual}}(y^*)|}{|J(x^*)|}, \quad (6)$$

where x^* and y^* are the current best solutions of the primal and dual problems, respectively, and J and J^* are the cost functions of the primal and dual problems, respectively. The MIP GAP ensures that we can assess the quality of the minimization during solution time and terminate the computation when the result is good enough (small enough MIP GAP). Furthermore, if the gap reaches 0 at any point, we are sure that the current solution is a global optimum.

4 Formulation of the Mixed Integer Quadratic Program

Recent works on high-dimensional confounding or deconfounding clarify the connections between distributional robustness, replicability, and causal inference [36, 18]. Distributional robustness differs significantly from traditional robust statistical methods [22, 19], which typically handle outliers in the training data, while our work focuses on evaluating the existence of a confounding factor.

In this section, we inherit from distributional robustness and present the formulation of the Mixed Integer Quadratic Program (MIQP) to infer the causal structure. Since we cannot observe all relevant variables, we must deal with the situation of hidden confounding. The problem is formalized in the following form corresponding to a structural equation model (SEM) [3, 29]:

$$Y_i \leftarrow X_i w_0 + g(H_i, A_i) + \epsilon_{Y,i},$$

where:

- $\epsilon_{Y,i}$ is the noise term, independent of all variables that appear "upstream" from Y_i .
- A_i is an exogenous variable, though not considered in the following sections.

- \leftarrow represents an algebraic equality, implying a structural causal relationship.

If non-zero components of the vector w_0 are correlated with certain components of X_i , these components are defined as causal X -variables for Y_i . This means:

$$w_{0,j} \neq 0 \iff X_i \text{'s } j\text{-th component is a causal variable.} \quad (7)$$

For the scenario that there are no exogenous variable perturbations, we describe this with a structural equation model (SEM) as follows:

$$Y_i \leftarrow X_i w_0 + H_i \delta + \epsilon_{Y,i}, \quad (8)$$

$$X_i \leftarrow H_i \gamma + \epsilon_{X,i}, \quad (9)$$

where $\epsilon_{X,i}$, $\epsilon_{Y,i}$ and H_i are mutually independent. X_i is the observed $p \times 1$ covariate vector. H_i is the unobserved $q \times 1$ confounding variable vector. Our goal is to infer the confounding-free regression parameter w_0 and stabilize the prediction of the relationship between Y and X .

4.1 Connecting to Causality

The causal parameter w_0 can be seen as minimizing the worst-case risk:

$$w_0 = \arg \min_w \max_{P \in \mathcal{P}} \mathbb{E}_P [(Y_i - X_i w)^2],$$

where \mathcal{P} is a class of distributions containing perturbations of the original distribution, including confoundings. This modeling highlights the inherent connection between causality and distributional robustness [11, 30, 34].

In this perspective, we present the formulation of the Mixed Integer Quadratic Program (MIQP) used to infer the causal structure, with a new binary matrix $B = [b_{j,k}] \in \{0, 1\}^{d \times d}$ introduced to account for relationships explained by confounding factors, alongside the weight matrix W and binary adjacency matrix E adopted from the ExDAG model [38]. Weight matrix W represents the model weights. Whenever a field in $W_{j,k}$ is non-zero, the respective value in either $E_{j,k}$ (directed edge) or $B_{j,k}$ is nonzero (bidirected edge). At the same time, we extend the existing formulation by introducing an additional binary input parameter $f_{j,k}$ for each pair of variables (j, k) , where $j \neq k$, indicating that there is no direct causal relationship between variables j and k , but j and k might have a common cofactor. This follows from the meaning of the edges in a MAG - \rightarrow edge implies a direct causal relationship but does not rule out a possible latent confounding, \leftrightarrow means no direct causal relationship. Formally, we define the *Directed Edge Matrix* E as

$$e_{j,k} = \begin{cases} 1, & \text{if } j \rightarrow k, \\ 0, & \text{otherwise,} \end{cases} \quad (10)$$

and the *Bidirected Edge Matrix* B as

$$b_{j,k} = \begin{cases} 1, & \text{if } j \leftrightarrow k, \\ 0, & \text{otherwise.} \end{cases} \quad (11)$$

The new input matrix F , is by the definition,

$$f_{j,k} = \begin{cases} 1, & \text{if } j \not\rightarrow k \text{ and } k \not\rightarrow j, \\ 0, & \text{otherwise.} \end{cases} \quad (12)$$

Based on the above assumptions, one can substitute algebraic equalities 9 into 8, and the work of [38] is extended as explained in the next section.

4.2 MILP Formulation

The cost function for the Mixed Integer Quadratic Program of ExMAG is the following l_p norm:

$$l_q = \sum_{i=1}^n \sum_{j=1}^d \left[X_{i,j} - \sum_{k=0; k \neq j}^d X_{i,k} w_{k,j} \right]^q + \lambda \sum_{j=0}^d \sum_{k=0}^d (e_{j,k} + b_{j,k}), \quad (13)$$

where:

- $X_{i,j}$ represents the value of the j -th variable for the i -th data point;
- $w_{k,j}$ represents the weight of the edge from variable k to variable j ;
- $e_{j,k}$ is the binary decision variable indicating the presence of a directed edge from j to k ;
- $b_{j,k}$ is the binary decision variable indicating the presence of a bidirected edge between j and k ;
- λ is a regularization parameter controlling the trade-off between the model fit and the edge penalty.
- The exponent $q \in \mathbb{N}$ can take values $q = 1$ or $q = 2$. While setting $q = 1$ leads to a mixed-integer linear program (MILP), which case would not correspond to the maximum likelihood estimator. If we choose $q = 2$, resulting in a mixed-integer quadratic problem (MIQP).

As in the ExDAG model, the weights are bounded by introducing a large constant c that ensures the weights are appropriately constrained when there is an edge between the variables. The bounding avoids bilinear terms in the cost function in (13). As a matrix form, the weight constraints can be restrained as:

$$\begin{aligned} -c \cdot (E + B) \leq W \leq c \cdot (E + B) & \quad (\text{Weight Constraint}) \\ E + B \leq \mathbf{1} & \quad (\text{Edge Constraint}) \end{aligned}$$

The (Edge Constraint) means that there cannot be a directed as well as a bidirected edge between the same two vertices. Additionally, we enforce that the bidirected matrix is symmetric, i.e.,

$$B = B^T. \quad (14)$$

If $f_{j,k} = 1$, then we know there is no direct causal relationship between j and k , and therefore, $e_{j,k} = 0$. Formally, this translates to condition

$$F + E \leq \mathbf{1}. \quad (15)$$

Inversely, $f_{j,k} = 0$ implies a directed edge rather than a bidirected edge between j and k . Therefore,

$$B \leq F. \quad (16)$$

Lastly, we must enforce conditions for directed or almost directed cycles and inducing paths. Those conditions are enforced lazily using a separation routine explained later. Directed cycles are enforced in a way adopted from [38]. Therefore, they are left out of this paper. Suppose an almost directed cycle is formed by edges in set E and a bidirected edge (x, y) . Then, this almost directed cycle is forbidden by constraint

$$b_{x,y} + \sum_{(j,k) \in E} e_{j,k} \leq |E|. \quad (\text{Acyclic Constraint})$$

Similarly, if there is an inducing path formed by path P that contains bidirected edges, and set E contains all directed edges that participate in the ancestor relationship (including multiple paths) between the inner points of the path and the terminals of P , this inducing path is forbidden by

$$\sum_{(j,k) \in P} b_{j,k} + \sum_{(j,k) \in E} e_{j,k} \leq |E| + |P| - 1. \quad (\text{Inducing Paths Constraint})$$

Note that the second condition does not necessarily eliminate the inducing path, as the optimizer might forbid one of the directed edges in E without influencing the ancestor relationship. This results in the path P being found in the next iteration, with a smaller set of directed edges, and the process is repeated.

By enforcing these constraints, we ensure that the MIQP correctly models the causal relationships between the variables while respecting the independence structure defined by $f_{j,k}$ and the potential confounding relationships captured by $b_{j,k}$.

5 Separation Routine for the Maximal Ancestral Graphs

The main contribution of this section is the separation routine that allows us to identify whenever a graph is not an instance of a maximal ancestral graph. To do so, we need to identify directed cycles, almost directed cycles, and inducing paths. The directed cycles can be found in $\mathcal{O}(d^2)$ using depth-first-search (DFS); such an approach can be found in [38]. For both inducing paths and almost directed cycles, we will use a distance matrix constructed on the graph of directed edges. Such distance matrix can be obtained using the Floyd-Warshall algorithm [16].

Once having the distance matrix, to check for almost directed cycles, we can iterate over all bidirected edges and test whether the distance between the endpoints is finite, i.e., we have a directed path connected by a bidirected edge. See Algorithm 1 for details.

Algorithm 1 Function to identify almost directed cycles.

Input: directed edges e , bidirected edges b

```

function ALMOST-DIRECTED-CYCLES( $e, b$ )
   $d \leftarrow$  DISTANCE-MATRIX( $e$ )
  for all  $j \in 1, 2, \dots, d$  do
    for all  $k \in 1, 2, \dots, d$  do
      if  $b_{j,k} == 1$  &  $d_{j,k} < \infty$  then
         $E =$  TRACE-DISTANCE-MATRIX( $d, e, j, k$ )
        Found cycle formed by edges  $E$  and  $j \leftrightarrow k$ 
      end if
    end for
  end for
end function

```

In the case of inducing paths, the problem is more complicated. We use DFS started from each of the vertices. Once started from vertex x , this DFS routine checks for all possible inducing paths that terminate in x . For efficiency, a set of all possible endpoints of the path is held. Once this set is empty, the DFS search is terminated, and no further exploration is performed. The set is updated using the distance matrix calculated from the graph of the directed edges. If we consider a vertex y , x must be either its ancestor (meaning that possible endpoints for y remain unchanged) or it is among the points that are reachable from y (meaning that the possible endpoints for y are replaced with their intersection with the set of all points reachable from y). See Algorithm 2 for details.

Once having the bidirected edges in the inducing paths and almost directed cycles, we need to trace back the Floyd-Warshall distance matrix to find all edges that form the cycle or the ancestor relationship. This is done using calls to the function in Algorithm 3.

If directed cycles, almost directed cycles, and inducing paths are found, the algorithm applies lazy constraints in Acyclic Constraint and in Inducing Paths Constraint. Otherwise, we know that the program converged to the optimum, and we have a maximal ancestral graph, which minimizes (13).

6 Experimental Evaluation

6.1 Used Datasets

We test the ExMAG algorithm on both synthetic and real-world datasets. The first synthetic dataset is based on the *Erdős-Rényi model* (ER) [13], in which the ground truth graph is randomly selected from all graphs with d vertices and m edges (parameter of the experiment, for example, dataset ER-5 contains 5 edges per variable, i.e., $m = 5 \cdot d$). The weights of the graph are randomly sampled from the set $(-2.0, -0.5) \cup (0.5, 2.0)$.

Once the ground truth model is created, then the training data are generated using the structural model equation 8, 9 (H_i set to 0). Then, 20% of variables are treated as latent variables and hidden from the training data. The respective columns and rows from the ground truth weight matrix W have also been removed. Finally, 20% of edges between variables not connected by an edge in the ground truth data are marked in F .

The second dataset uses randomly generated *bow-free* (BF) graphs, a subset of all possible MAGs. A bow-free graph is defined as a graph that does not contain a pair of vertices i, j , such that $i \rightarrow j$ and at the same time $i \leftrightarrow j$. The BF graph generation process has two parameters. First, the probability

Algorithm 2 Function that identifies inducing paths.

Input: directed edges e , bidirected edges b

```
function INDUCING-PATHS( $e, b$ )
   $d \leftarrow$  DISTANCE-MATRIX( $e$ )
  for all  $j \in 1, 2, \dots, d$  do
    INDUCING-PATHS-DFS( $d, e, b, j, j, \{1, 2, \dots, d\}, [j]$ )
  end for
end function
function INDUCING-PATHS-DFS( $d, e, b, start, u, possible\ endpoints, path$ )
  if possible endpoints are empty then return
  end if
  if LEN( $path$ ) > 2 &  $u$  in possible endpoints then
    FOUND-INDUCING-PATH( $d, e, path$ )
  end if
  for all  $v \in 1, 2, \dots, d$  such that  $e_{u,v} = 1$  do
    if  $d_{v,start} < \infty$  then  $v$ -endpoints = possible endpoints
    else  $v$ -endpoints = possible endpoints  $\cap \{x \mid d_{v,x} < \infty\}$ 
    end if
    INDUCING-PATHS-DFS( $d, e, b, start, v, v$ -endpoints,  $path+v$ )
  end for
end function
function FOUND-INDUCING-PATH( $d, e, P$ )
   $E = \{\}$ 
  for all vertices  $j \in P$  and  $j \notin \{P_0, P_{|P|}\}$  do
     $E = E \cup$  TRACE-DISTANCE-MATRIX( $d, e, j, P_0$ )
     $E = E \cup$  TRACE-DISTANCE-MATRIX( $d, e, j, P_{|P|}$ )
  end for
  Found inducing path formed by path  $P$  and directed edges  $E$ 
end function
```

Algorithm 3 Functions that help in the separation routine.

Input: distances d defined by directed edges e , start point j , and endpoint k

Output: edges on any path from j to k

```
function TRACE-DISTANCE-MATRIX( $d, e, j, k$ )
  if  $d_{j,k} == \infty$  then return
  end if
  visited =  $\{(j, k)\}$ 
  stack = stack with  $(j, k)$ 
  edges =  $\{\}$ 
  while stack is not empty do
     $u, v \leftarrow$  POP(stack)
    for all  $w \in 1, 2, \dots, d$  s.t.  $d_{u,w} + d_{w,v} < \infty$  do
      visited  $\leftarrow$  visited  $\cup \{(u, w), (w, v)\}$ 
      if  $e_{u,w}$  then edges  $\leftarrow$  edges  $\cup \{(u, w)\}$ 
      else if  $e_{w,v}$  then edges  $\leftarrow$  edges  $\cup \{(w, v)\}$ 
      end if
      add  $\{(u, w), (w, v)\}$  to stack
    end for
  end while
end function
```

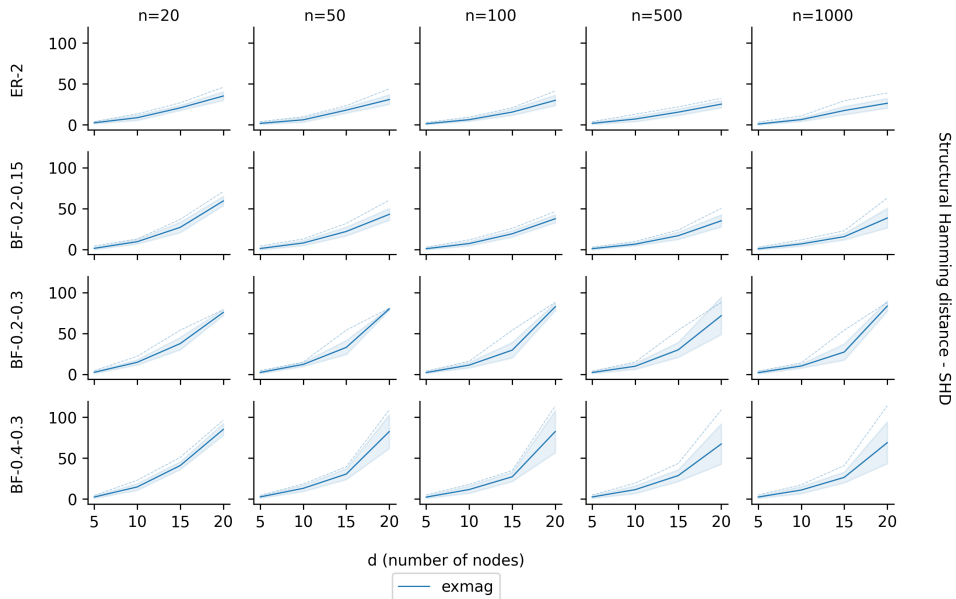


Figure 1: SHD values (in the vertical axis) for different settings of d (in the horizontal axis) and n (horizontal choice of the graph). The plots in the vertical dimension differ according to the dataset used. The channel shows the variance of the results for different choices of seed. See supplementary materials for results on more datasets.

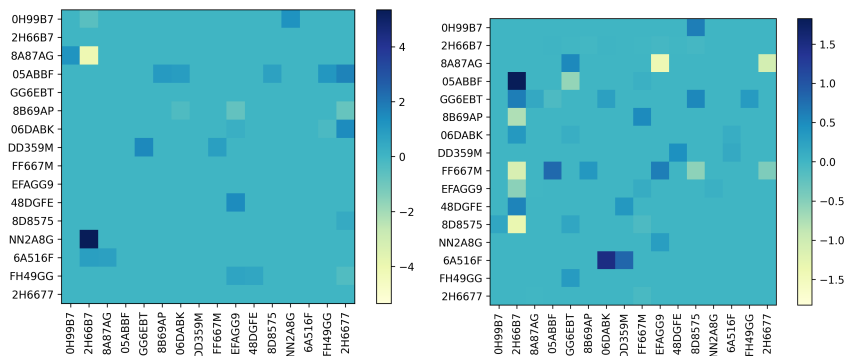


Figure 2: Heatmap of weight matrix W (left) and bidirectional weight matrix W (right) on the financial dataset.

of a directed edge. Second, the probability of bidirected edge. The generation process is as follows. First, a bow-free graph with the given edge probabilities is generated randomly. The weights of the sampled graphs are randomly sampled from the set $(-2.0, -0.5) \cup (0.5, 2.0)$. The adjacency matrix of the directed edges defines the weights of the structural equation model. Then the data samples are generated using the structural equation, where the noise is sampled from multivariate Gaussian distribution with covariance matrix equals to the adjacency matrix of bidirected edge generated in the previous step.

The third dataset uses real-world data from the *financial* sector. Paper [1] works with systemic credit risk, one of the most important concerns within the financial system, using dynamic Bayesian networks. The data show that transport and manufacturing companies are likely to transfer risk to other sectors, while banks and the energy sector are likely to be influenced by the risks from other sectors. The data from [1] contains a 10-time series capturing the spreads of 10 European credit default swaps (CDS), and further six time series are added from [37].

We set matrix F to encode for no direct causal relationship between any two pairs of companies from different sectors. Banks sector includes 48DGF, 05ABBF, 8B69AP, 06DABK, EFAGG9, 2H6677, FH49GG, and 8D8575. Insurance sector includes GG6EBT, DD359M, and FF667M. And lastly, transportation sector and manufacturing includes 0H99B7, 2H66B7, 8A87AG, NN2A8G, and 6A516F.

6.2 Evaluation Criteria

Suppose that a tested algorithm produced weight matrix W . Such a matrix can contain nearly zero weights. For such reasons, thresholding is done, keeping only edges with weight greater or equal to δ . In cases when the ground-truth weight matrix W is known, the best solution (in terms of structural Hamming distance, see below) is kept over those defined by different threshold δ values.

In the evaluation, we use the *structural Hamming distance (SHD)*. This distance is the sum of contributions over all pairs of variables in the graph. For two variables i, j , let $GT \in \{\rightarrow, \leftarrow, \leftrightarrow, \emptyset\}$ be the edge type in the ground truth graph and $PR \in \{\rightarrow, \leftarrow, \leftrightarrow, \emptyset\}$ be edge type in the predicted graph. Then the contribution of i, j pair to SHD is

$$r_{ij} = \begin{cases} 0, & \text{if } GT = PR, \\ 0.5, & \text{if } GT \neq PR \text{ and } GT \neq \emptyset \text{ and } PR \neq \emptyset, \\ 1, & \text{otherwise.} \end{cases}$$

Other measured criteria include *runtime* and *F1-score*, i.e., the harmonic mean of precision and recall.

6.3 Experiment Setting

In the experiments, we show the results of ExMAG. In the case of synthetic datasets, we generated random graphs with $d \in \{5, 10, 15, 20, 25\}$. The number of samples was in $n \in \{20, 50, 100, 500, 1000\}$, and ground-truth graph edge ratio was in $\{2, 3, 4, 5, 6, 7, 8, 9, 10, 15, 20\}$ percent. Both tested algorithms were run 10 times, each time with a different seed value and the results were then averaged.

6.4 Experimental Results

The SHD results is shown in Fig. 4 and in the supplementary materials on more datasets. The plots show a comparison of SHD values for ExMAG on both synthetic datasets. As can be seen, the structural Hamming distance grows with the number of variables and decreases with the number of samples. For results with the F1-score, visit the supplementary materials. The results show that the F1 score is close to 1, with the score increasing with the higher number of samples and decreasing with the higher number of variables.

The results on the real-world dataset can be seen in 2. Contrary to the original expectations, the highest risk importer is company 2H66B7, which stands for Lufthansa. The second highest risk importer is 2H6677, i.e., the Deutsche Bank, which is an expected result.

7 Conclusion

Learning of Dynamic Bayesian networks has received considerable attention as a means of causal learning. With a few exceptions, the research has not considered confounding explicitly. Our method, ExMAG, estimates a maximally ancestral graph, capturing confounding and causal relationships using bidirected and directed edges of a mixed graph. The method provides state-of-the-art statistical performance.

The predictive power of forecasting with variants of dynamical Bayesian networks with confounding considerations is an important direction for further work. While it seems clear that (1) even in dynamical Bayesian networks, marginalization is hard, and thus the computational complexity may be high, (2) the statistical performance should improve by considering the confounding.

Acknowledgements

This work has been partially supported by the CoDiet project, co-funded by the European Union under Horizon Europe grant number 101084642.

This work has been partially supported by project MIS 5154714 of the National Recovery and Resilience Plan Greece 2.0 funded by the European Union under the NextGenerationEU Program.

Disclaimer

This paper was prepared for information purposes and is not a product of HSBC Bank Plc. or its affiliates. Neither HSBC Bank Plc. nor any of its affiliates make any explicit or implied representation or warranty

and none of them accept any liability in connection with this paper, including, but not limited to, the completeness, accuracy, reliability of information contained herein and the potential legal, compliance, tax or accounting effects thereof. Copyright HSBC Group 2025.

References

- [1] Laura Ballester, Jesúa López, and Jose M. Pavía. European systemic credit risk transmission using bayesian networks. *Research in International Business and Finance*, 65:101914, 2023.
- [2] Pietro Belotti, Christian Kirches, Sven Leyffer, Jeff Linderoth, James Luedtke, and Ashutosh Mahajan. Mixed-integer nonlinear optimization. *Acta Numerica*, 22:1–131, 2013.
- [3] K.A. Bollen. *Structural Equations With Latent Variables*, volume 210. John Wiley & Sons, 1989.
- [4] Pierre Bonami, Mustafa Kılınç, and Jeff Linderoth. *Algorithms and Software for Convex Mixed Integer Nonlinear Programs*, volume 154. 10 2009.
- [5] Peter Bühlmann. Invariance, causality and robustness. *Statistical Science*, 35(3):404–426, 2020.
- [6] Peter Bühlmann and Domagoj Čevd. Deconfounding and causal regularisation for stability and external validity. *International Statistical Review*, 88:S114–S134, 2020.
- [7] Peter Bühlmann and Sara Geer. *Statistics for High-Dimensional Data: Method, Theory and Applications*. 01 2011.
- [8] Domagoj Cevd, Peter Bhlmann, and Nicolai Meinshausen. Spectral deconfounding for causal inference. *Annals of Statistics*, 46(6B):3313–3340, 2018.
- [9] Tom Claassen and Ioana G. Bucur. Greedy equivalence search in the presence of latent confounders. In *Proceedings of the 38th Conference on Uncertainty in Artificial Intelligence (UAI)*, 2022.
- [10] R. J. Dakin. A tree-search algorithm for mixed integer programming problems. *Comput. J.*, 8:250–255, 1965.
- [11] A. P. Dawid and V. Didelez. Causal inference in graphical models. *Journal of Causal Inference*, 2(1):22–38, 2010.
- [12] Alberto Del Pia, Santanu Dey, and Marco Molinaro. Mixed-integer quadratic programming is in np. *Mathematical Programming*, 162, 07 2014.
- [13] P Erdős and A Rényi. On random graphs i. *Publ. math. debrecen*, 6(290-297):18, 1959.
- [14] Robin J. Evans. Model selection and local geometry. *The Annals of Statistics*, 48(6):3513 – 3544, 2020.
- [15] Jianqing Fan, Zijian Guo, Ning Hao, and Zijian Ren. Estimating false discovery proportion under arbitrary covariance dependence. *Journal of the American Statistical Association*, 115(531):1530–1546, 2020.
- [16] Robert W. Floyd. Algorithm 97: Shortest path. *Commun. ACM*, 5(6):345, June 1962.
- [17] Yoav Gilad and Orna Mizrahi-Man. A reanalysis of mouse encode comparative gene expression data. *F1000Research*, 4, 05 2015.
- [18] Zijian Guo, Domagoj Čevd, and Peter Bühlmann. Doubly debiased lasso: High-dimensional inference under hidden confounding. *Annals of statistics*, 50(3):1320, 2022.
- [19] F. R. Hampel et al. Robust statistics. *Wiley-Interscience*, 18, 1986.
- [20] Z. Hu. Causal discovery with ancestral graphs. 2023.
- [21] Zhenyu Hu and Robin J. Evans. Faster algorithms for markov equivalence. In *Proceedings of the 36th Conference on Uncertainty in Artificial Intelligence (UAI)*, 2020.
- [22] P. J. Huber. Robust estimation of a location parameter. *Annals of Mathematical Statistics*, 35(1):73–101, 1964.
- [23] Guido W. Imbens. Instrumental Variables: An Econometrician’s Perspective. *Statistical Science*, 29(3):323 – 358, 2014.

- [24] Jan Kronqvist, Andreas Lundell, and Tapio Westerlund. The extended supporting hyperplane algorithm for convex mixed-integer nonlinear programming. *Journal of Global Optimization*, 64, 06 2015.
- [25] Clifford Lam and Qiwei Yao. Factor modeling for high-dimensional time series: inference for the number of factors. *The Annals of Statistics*, pages 694–726, 2012.
- [26] Shin Lin, Yiing Lin, Joseph R. Nery, Mark A. Urich, Alessandra Breschi, Carrie A. Davis, Alexander Dobin, Christopher Zaleski, Michael A. Beer, William C. Chapman, Thomas R. Gingeras, Joseph R. Ecker, and Michael P. Snyder. Comparison of the transcriptional landscapes between human and mouse tissues. *Proceedings of the National Academy of Sciences*, 111(48):17224–17229, 2014.
- [27] Maya B. Mathur and Tyler J. VanderWeele. Methods to address confounding and other biases in meta-analyses: Review and recommendations. *Annual Review of Public Health*, 43(Volume 43, 2022):19–35, 2022.
- [28] Richard McElreath. *Statistical Rethinking: A Bayesian Course with Examples in R and Stan*. 01 2018.
- [29] Judea Pearl. *Causality: Models, Reasoning, and Inference*. Cambridge University Press, Cambridge, 2009.
- [30] J. Peters et al. *Elements of Causal Inference*. MIT Press, 2016.
- [31] Joseph Ramsey, Peter Spirtes, and Jiji Zhang. Adjacency-faithfulness and conservative causal inference. In *Proceedings of the Twenty-Second Conference on Uncertainty in Artificial Intelligence*, UAI’06, page 401–408, Arlington, Virginia, USA, 2006. AUAI Press.
- [32] Thomas S. Richardson. A factorization criterion for acyclic directed mixed graphs. In *Proceedings of the 25th Conference on Uncertainty in Artificial Intelligence (UAI)*, pages 462–469, 2009.
- [33] Thomas S. Richardson and Peter Spirtes. Ancestral graph markov models. *The Annals of Statistics*, 30(4):962–1030, 2002.
- [34] M. Rojas-Carulla et al. Causal inference and distributional robustness. *Statistical Science*, 33(3):432–445, 2018.
- [35] Paul Rosenbaum. *The Central Role of the Propensity Score in Observational Studies for Causal Effects*, pages 170–184. 09 2006.
- [36] Dominik Rothenhäusler, Nicolai Meinshausen, Peter Bühlmann, and Jonas Peters. Anchor regression: heterogeneous data meets causality. *Journal of the Royal Statistical Society: Series B (Statistical Methodology)*, 80(5):1101–1122, 2018.
- [37] Pavel Rytir, Ales Wodecki, Georgios Korpas, and Jakub Marecek. Exdbn: Exact learning of dynamic bayesian networks, 2024.
- [38] Pavel Rytír, Aleš Wodecki, and Jakub Mareček. Exdag: Exact learning of dags. *arXiv preprint arXiv:2406.15229*, 2024.
- [39] Peter Spirtes, Clark Glymour, and Richard Scheines. *Causation, Prediction, and Search, 2nd Edition*. 01 2000.
- [40] Tapio Westerlund and Frank Pettersson. An extended cutting plane method for solving convex minlp problems. *Computers and Chemical Engineering*, 19:131–136, 1995. European Symposium on Computer Aided Process Engineering 3-5.

A F1-score Results

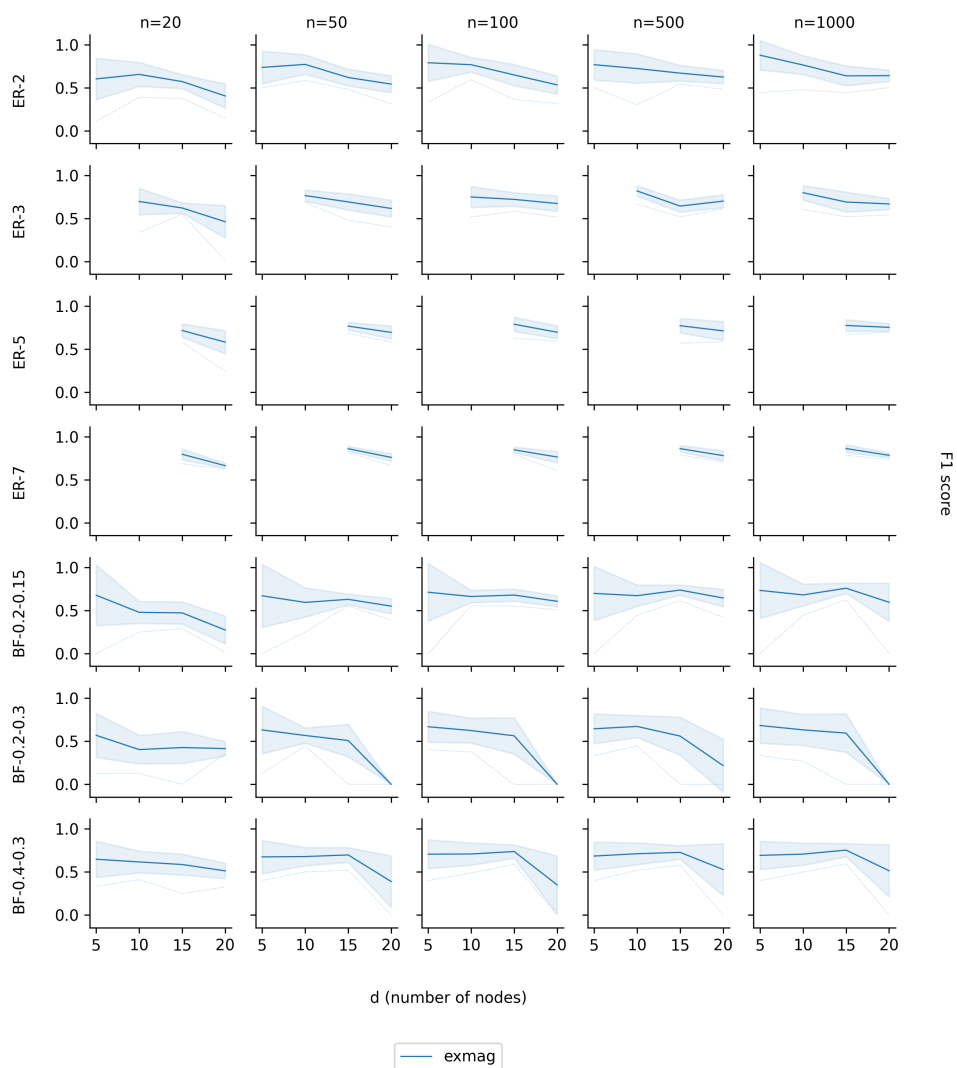


Figure 3: F1-score (in the vertical axis) for different settings of d (in the horizontal axis) and n (horizontal choice of the graph). The plots in the vertical dimension differ according to the dataset used. The channel shows the variance of the results for different choices of seed. Please note that for some of the ER plots, the graphs can be generated only for higher numbers of variables. For example, there exists no ER-5 with $d = 10$, as it would need to contain 50 edges, while maximum is 45.

B SHD Results

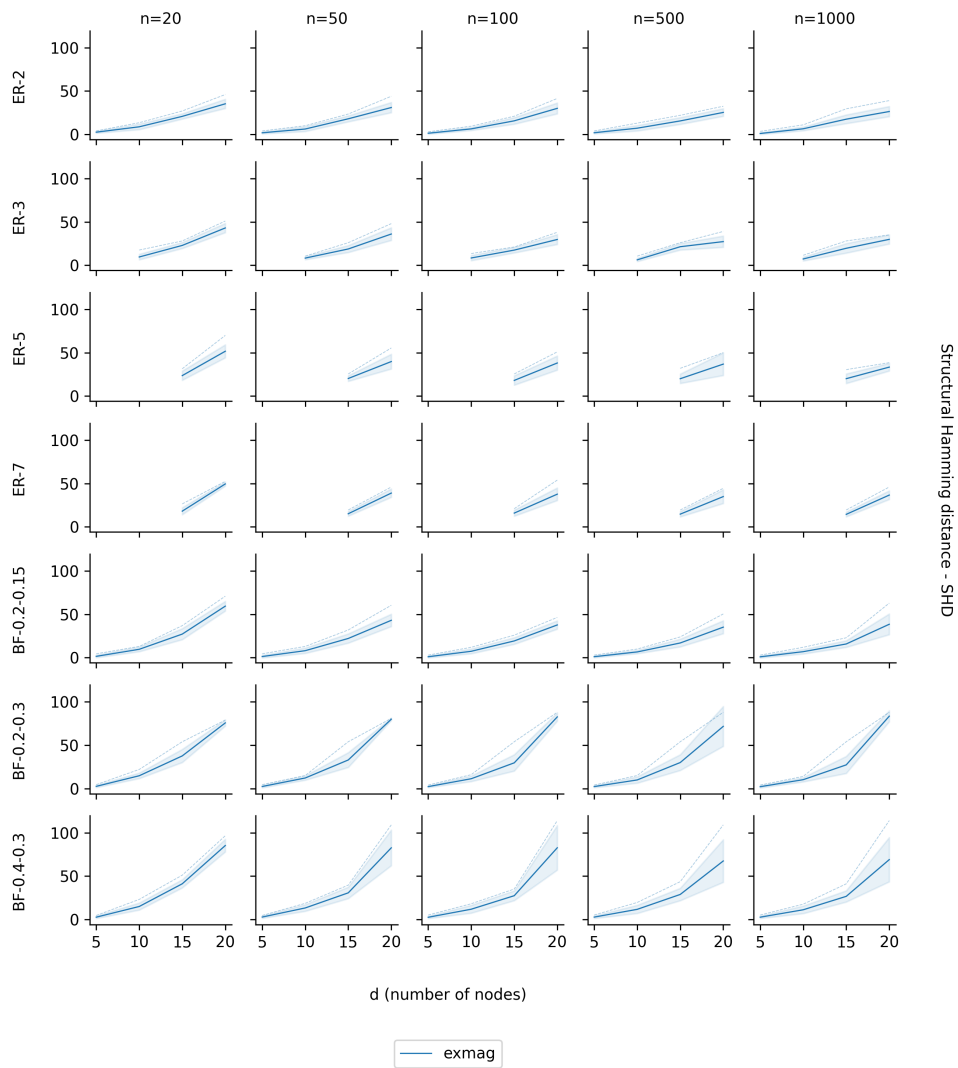


Figure 4: SHD values (in the vertical axis) for different settings of d (in the horizontal axis) and n (horizontal choice of the graph). The plots in the vertical dimension differ according to the dataset used. The channel shows the variance of the results for different choices of seed.